Sway Model for the Lateral Torsional Buckling Analysis of Wooden Twin-Beam-Deck Systems

By Yang Du [a], Magdi Mohareb [b], and Ghasan Doudak [c]

[a] Department of Civil Engineering, University of Ottawa, Ottawa, ON, Canada, K1W6N5. Email: ydu082@uottawa.ca

[b] Department of Civil Engineering, University of Ottawa, Ottawa, ON, Canada, K1W6N5 (corresponding author). Email: mmohareb@uottawa.ca

[c] Department of Civil Engineering, University of Ottawa, Ottawa, ON, Canada, K1W6N5. Email: gdoudak@uottawa.ca

Abstract

The present study develops a finite element model for the lateral torsional buckling analysis of wooden twin beams braced by deck boards subjected to gravity or wind uplift loading. The restraining action of the deck boards is modelled as continuous partial lateral and twist restraints provided at the top of both beams that capture the interaction between both beams. A parametric study is then conducted to examine the effects of beam and deck spans, load type, load height, lateral restraint height and stiffness and number of beam spans on the overall buckling capacity. The results indicate that the restraining effects of deck boards significantly improve the lateral torsional buckling capacity of twin-beam-deck assemblies.

Author Keywords

Lateral torsional buckling; wooden beam-deck system; finite element analysis; lateral restraint; twist restraint

This article is to be cited as: Du Y., Mohareb M, Doudak D (2019) Sway Model for the Lateral Torsional Buckling Analysis of Wooden Twin-beam-deck Systems, Structures, 19: 19-29.

The copy-edited version of this article is available at: https://doi.org/10.1016/j.istruc.2018.11.012

1. Introduction

Timber floor and roof systems often consist of a set of relatively deep rectangular beams braced at the top by tongue-and-groove wooden deck boards through nail connections. While deep beams provide efficient means of material usage in bending, they are prone to lateral torsional buckling (LTB) as a possible mode of failure. Deck boards can potentially improve the buckling capacity of such systems by partially restraining the twist and relative lateral displacements between the parallel beams. Despite the common use of such systems in timber structures, contemporary design standards (NDS [1], CAN/CSA O86 [2], Eurocode 5 [3]) recognize the beneficial role of deck boards in suppressing LTB of beams when deck boards prevent the lateral displacement along the beams' compression edge, but do not provide design guidelines for determining the LTB capacity of wooden beams where (1) the tension edge is restrained as may be the case for wind uplift on roof beams, or where (2) the deck boards provide partial lateral and/or twist restraints for beams subjected to gravity loads. In this context, the present study aims to develop a finite element solution for the LTB analysis of timber beam-deck systems that incorporates (1) the characteristics of nailed joints in providing partial lateral restraint, and (2) the beneficial effect of partial twist restraint provided by the deck boards to the beams. Unlike previous LTB studies which treat each beam separately while idealizing the effect of deck boards using lateral or rotational springs, the present study treats both beams and the deck boards as an integrated system that naturally captures the interaction between all three components throughout LTB, while keeping the computational and modelling effort to a minimum. A pilot study on twin-beam-deck systems (Du et al. [4]) based on ABAQUS showed that non-sway models have a propensity buckle under net wind uplift but not under gravity loads, while sway models can buckle under net wind uplift and gravity. Analytical and numeric models

for non-sway LTB were then formulated in (Du et al. [5]). The present study complements past work by developing a finite element formulation for the LTB of twin-beam-deck systems that captures the sway effects.

2. Literature Review

Consistent with the objective of the present study, a review is firstly presented for the LTB literature for wood beams, followed by a review of stability research on continuously restrained beams under wind and gravity loading. In general, continuously restrained beams can be categorized into sway models, whereby the beams are free to move laterally, and non-sway models where beams are fully restrained from lateral movements at deck level. Since a recent review of non-sway models has been presented in Du et al. [5], only research pertaining to sway models is presented herein. Finally, a review of past research related to the strength and stiffness requirements for continuous restraints is provided.

2.1 Overview of stability research on wood members

Past research on the LTB of wood beams has primarily focused on single beams and on comparing test results against the classical LTB solution or relevant design standard provisions. This includes the work of Hooley and Madsen [6] who developed design equations for elastic and inelastic LTB of rectangular beams and verified those equations experimentally. Hindman et al. [7] experimentally tested the LTB capacity of unbraced rectangular cantilevers and compared test results with design standard provisions. In a subsequent study, Hindman et al. [8] expanded their study to composite I-joists. Burow et al. [9] and Burow et al. [10] evaluated the adequacy of LTB design equations by testing simply-supported and cantilevered composite I-joists with a wide range of slenderness ratios. Xiao [11] conducted a full-scale experimental investigation on the elastic LTB of simply-supported beams with rectangular cross-section. A 3D

finite element model was also developed to study the sensitivity of material properties and the effects of load height and boundary support height on the LTB capacity. St-Amour [12] experimentally investigated the LTB of simply-supported composite I-joists and developed an eigenvalue 3D finite element analysis (FEA) model for straight beams, and a non-linear FEA model for beams with initial imperfections. Hu et al. [13] and Hu et al. [14] developed lateral buckling solutions for wood beams with rigid and flexible mid-span lateral braces offset from the shear center. However, none of the above studies considered beams with continuous bracing. Such systems have been studied by Zahn [15] who formulated the equilibrium equations governing the behavior of rectangular beams partially restrained by the diaphragm action of deck boards. The solution was experimentally verified by Jenkinson and Zahn [16] against the results of a full-scale LTB test for a system consisting of two beams joined by deck boards and subjected to uniform moments. An energy formulation was also developed by Zahn [17] for the LTB of a single beam within a floor system by accounting for the internal strain energy within the tributary decking strip of the beam. In summary, except for the study of Jenkinson and Zahn [16], past experimental LTB studies on wood beams have focused on individual beams as opposed to beam-deck systems.

2.2 Sway models under gravity load

Vlasov [18] formulated the general differential equations for a beam embedded in an elastic medium and subjected to uniform moment loading. The critical moment was determined for a beam continuously braced along its span through elastic lateral and twist restraints. Pincus and Fisher [19] developed a LTB solution for twin beams braced by a shear diaphragm and subjected to uniform moments. The solution captured the shear and twist actions of the steel diaphragm. Errera et al. [20] extended the solution of Pincus and Fisher [19] to other bracing scenarios. Floor assemblies consisting of two

beams laterally braced at their compression edge by the diaphragm shear action were investigated by Apparao [21] who developed an eigen-value buckling solution for straight beams and a nonlinear load-deformation solution for beams with initial imperfections. Hancock and Trahair [22] formulated a finite element solution for continuously braced beam-columns which characterized the deck action as elastic restraints that partially restrain lateral displacement, twist along beam longitudinal axis, weak-axis rotation and warping of the member. A closed-form solution was also developed by Trahair [23] for beam-columns under constant loading. Assadi and Roeder [24] investigated the stability of cantilevers with elastic lateral restraint at the top edge. Albert and Dawe [25] developed a finite element solution for the buckling analysis of a two-span I-section beam whose top flange is restrained by elastic lateral and twist springs. For the purpose of capturing the interaction between the web and flanges, the flanges were modelled by one-dimensional beam elements while the web was modelled by plate elements. The inelastic behavior was captured by omitting yielded zones in the beam. Khelil and Larue [26] developed an energy-based solution for simply-supported beams with continuous partial lateral restraint. The solution was able to predict the buckling capacity for beams with uniform and non-uniform moment distributions.

2.3 Sway models under wind uplift

Studies on sway models with relatively low self-weight and subjected to net wind uplift include the work of Pekoz and Soroushian [27] developed a buckling solution for steel purlins restrained by sheeting through modelling the systems as beams on elastic foundation. The problem was also investigated by Sokol [28] who idealized the purlin-sheeting systems as columns on elastic rotational foundation. Lucas et al. [29] formulated a non-linear elasto-plastic finite element model with geometric nonlinearity.

126 The model captured the interaction between purlins and sheeting, cross-sectional
127 distortion and local buckling effects. In a subsequent study, Lucas et al. [30] developed
128 a simplified model where the sheeting was idealized as elastic springs. Ye et al. [31]
129 adopted a finite strip model to investigate the local, distortional and lateral torsional
130 buckling of zed-purlins restrained by sheeting. The LTB of steel purlins laterally braced
131 by sheeting was investigated by Chu et al. [32], Li [33] and Chu et al. [34]. Basaglia et
132 al. [35] developed a solution for local, distortional and lateral torsional buckling of
133 channel and zed purlins restrained by steel sheeting. Apart from Sokol [28], Chu et al.
134 [32], Li [33], and Chu et al. [34], the above studies have focused on local or distortional
135 buckling of purlins. A common aspect among the above studies is that they were aimed
136 at steel purlin-sheeting systems. In contrast, the present study develops a LTB finite
137 element solution that tackles aspects specific to wooden beam-to-deck connections.

138 **2.4 Strength and stiffness requirements for continuous restraints**

139 Based on the studies of Errera et al. [20] and Apparao [21], Nethercot and Trahair [36]
140 as well as Errera and Apparao [37] proposed simplified design equations for the critical
141 loads of a single beam continuously braced by a shear diaphragm under uniform
142 moment loading. The stiffness requirement of the diaphragm to achieve desired moment
143 resistance was developed. The strength requirement was also proposed for initially
144 crooked beams. Starting from the models of Hancock and Trahair [22] and Trahair [23],
145 Trahair and Nethercot [38] added discrete restraint features to assess the effects of type
146 of continuous and discrete restraints on the buckling capacity of beam-columns.
147 Lawson and Nethercot [39] proposed a critical moment equation for a single beam
148 continuously braced by shear diaphragm. The solution incorporated moment gradient
149 and load height effects. Also developed were criteria to assess the adequacy of the
150 diaphragm shear stiffness. Helwig and Frank [40] developed a finite-element model for

151 the stability of twin-beam systems with sheeting acting as a shear diaphragm at the
152 beams' top edges. The authors confirmed the validity of the design equations proposed
153 by Nethercot and Trahair [36] for beams under uniform moments, and proposed
154 equations that account for loading heights. Also proposed was the diaphragm shear
155 stiffness required to achieve the design moment resistance. Helwig and Yura [41]
156 proposed a moment gradient equation for beams with stocky webs and suggested the
157 optimal diaphragm shear stiffness for beams with initial imperfections. In a later study,
158 Helwig and Yura [42] quantified the forces in shear diaphragms and outlined a
159 procedure for the design of shear diaphragms.

160 **2.5 Summary of literature**

161 Among the analytical solutions for the stability of continuously braced beams, the
162 studies of Vlasov [18], Albert and Dawe [25], Ye et al. [31], Li [33], and Basaglia et al.
163 [35] focused on the buckling of a single beam with continuous lateral and twist
164 restraints. In contrast, the present study tackles beam-deck systems. Analytical
165 solutions for the LTB of beam-deck systems consist of the work of Pincus and Fisher
166 [19], Errera et al. [20], Apparao [21], and Du et al. [5]. However, Pincus and Fisher
167 [19], Errera et al. [20] and Apparao [21] modelled the deck restraint through separate
168 rotational springs which do not fully capture the interaction between the two beams.
169 The study of Du et al. [5], while accounting for the interaction between both beams,
170 omitted the lateral sway effects. Another distinctive feature of the present study is that
171 it captures the partial relative lateral restraint between both beams provided by the wood
172 deck and the nailed connections, a feature absent in the work of Pincus and Fisher [19],
173 Errera et al. [20], Apparao [21] and Du et al. [5].

3. Constitutive Properties of Wood

Wood can be idealized as orthotropic with different mechanical properties in longitudinal (*L*), radial (*R*) and tangential (*T*) directions. For a wood member, the longitudinal axis is parallel to the grain, the radial axis is perpendicular to the grain and normal to the growth rings, and the tangential axis is perpendicular to the grain but tangent to the growth rings. Orthotropic constitutive behavior is characterized by twelve properties: three moduli of elasticity in the longitudinal, radial, and tangential directions, three shear moduli, and six Poisson's ratios. The moduli of elasticity and Poisson's ratios are interrelated (e.g., FPL [43]), which reduces the number of independent material properties to nine constants. Isopescu et al. [44] reported that the difference between properties in radial and tangential directions is insignificant in most wood species, thus reducing the number of independent properties to six. When no distinction is made between properties in radial and tangential directions, the circular orthotropy of wood coincides with rectangular orthotropy. Xiao et al. [45] conducted a LTB sensitivity analysis for wood beams using a 3D finite element model within the commercial software ABAQUS. Material was considered as orthotropic with six independent constants. The study showed that only the modulus of elasticity E_L in the longitudinal direction and the transverse shear modulus $G_T = G_{LR} = G_{LT}$ influence the LTB capacity. Other material properties $E_T = E_R, G_{RT}, \mu_{LR} = \mu_{LT}, \mu_{RT}$ were shown to have nearly no influence on the critical moments. Changes in these properties from the default values by ±50% resulted in differences of less than 1% in the critical moment predicted. The findings are also consistent with the observation from Hooley and Madsen [6] and with the critical moment equation in Eurocode 5 [3] which depends only on two constants E and G. The observation suggests some similarity with isotropic beams where the elastic LTB capacity is characterized only by the modulus of

elasticity and the shear modulus. Nevertheless, isotropic beams differ from wood orthotropic beams in that while the former has a G/E ratio ranging between 1/3 and 1/2, the later has a significantly lower G/E ratio in the neighborhood of 1/16.

4. Assumptions

The following assumptions have been adopted:

1. The formulation captures warping effects. While the study primarily targets beams with rectangular sections for which warping has a small contribution, the model remains equally valid for other doubly symmetric sections with more pronounced warping effects.
2. Beam and deck materials are assumed linearly elastic. As discussed under Section 3, the orthotropic behavior of wood is characterized by six constants E_L, $E_T = E_R$, $G_L = G_{LR} = G_{LT}$, G_{RT}, $\mu_L = \mu_{LR} = \mu_{LT}$ and μ_{RT}. Further, in the beam formulation sought, since the normal stresses in the radial and tangential directions are negligible compared to longitudinal stresses, the associated Young's moduli $E_T = E_R$ will not contribute to the internal strain energy expression. Also, given that the stress state in the beam is uniaxial, Poisson's ratios $\mu_{LR}, \mu_{LT}, \mu_{RT}$ will not influence the internal strain energy. Finally, as the shear stresses acting on the radial and tangential directions are negligible, the associated shear modulus G_{RT} does not appear in the strain energy expression. In summary, of the six orthotropic constitutive constants, only the modulus of elasticity in the longitudinal direction E_L and shear modulus G_T will appear in the internal strain energy expression, in a manner similar to isotropic materials.
3. Relative lateral displacements between beams and deck boards at the nailed joints are allowed in order to account for the flexibility of connections. Deck boards are

assumed to provide partial relative lateral restraint due to the combined flexibility of the nailed joints and deck boards (deck-joint assembly).

4. At each beam-deck joint, the deck board is assumed to rotate by the same angle of twist for the beam (i.e., fully fixed connection is assumed). Consequently, deck boards are assumed to provide continuous partial twist restraint to the beams.
5. The in-plane elastic shear restraint provided by the deck boards is negligible.
6. Throughout deformation, beam cross-sections remain rigid in their own plane, i.e., distortional effects are neglected.
7. Shear deformation effects within the beams are negligible, and
8. Pre-buckling deformation effects are omitted.

5. Formulation

5.1 Problem description and notation

The beam-deck system considered consists of two rectangular beams connected to deck boards through nails. Fig. 1 shows a cross-sectional view of the twin-beam-deck assembly. A left-hand coordinate system is used, with the z-axis oriented along the longitudinal direction of the beam, and the *x* and *y* axes taken in the plane of the cross-section. The positive sign convention adopted is consistent with that in Trahair [46] where the angle of twist is clockwise. A transverse load $q(z)$ is assumed to be applied to both beams at a distance $h(z)$ from the beam shear center. Under the external loads, the system undergoes vertical displacement $v_p(z)$ in going from Configuration 1 to 2, in which subscript p denotes the pre-buckling displacements. The applied loads are then assumed to be increased by a factor λ to attain the threshold value $\lambda q(z)$ at the onset of buckling (Configuration 3). Under the load increase, pre-buckling

247 deformations are assumed to linearly increase to $\lambda v_p(z)$. The system then undergoes
248 LTB as manifested by lateral displacements $u_1(z), u_2(z)$ and angles of twist $\theta_1(z)$,
249 $\theta_2(z)$ (Configuration 4) where subscripts 1,2 respectively denote the field variables
250 of the left and right beams. $u_1(z), u_2(z), \theta_1(z), \theta_2(z)$ are drawn in the positive
251 directions. In Fig. 1, points *B* and *D* are located at the deck underside and initially
252 coincide with points *A* and *C* located at the beams' top. At the onset of buckling, point
253 *A* at the top of beam 1 is assumed to undergo a lateral displacement u_A that differs
254 from that of point *B* at the deck underside. Also, point *C* located at the top of beam 2
255 undergoes a lateral displacement u_C which is different from that of point *D*, resulting
256 in a relative displacement between the top of both beams. The magnitude of relative
257 displacement depends on the lateral stiffness of the nailed joints, the axial and flexural
258 stiffness of the deck boards, including the effect of eccentricity between the deck board
259 centerline and beam-deck interface.

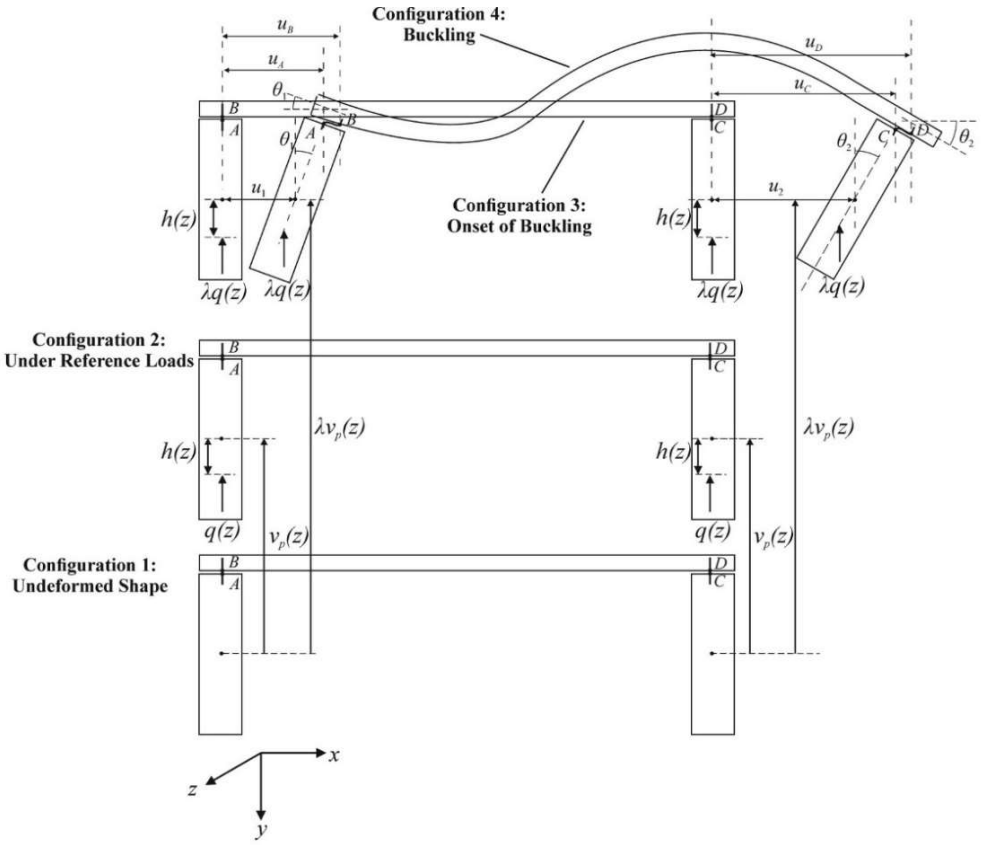

Fig. 1 Different stages of deformation

5.2 Total potential energy

The total potential energy Π of the twin-beam-deck system is

$$\Pi = U + V \tag{1}$$

in which U is the internal strain energy and V is the load potential energy. In Eq. (1), the internal strain energy has four contributions $U = U_{b1} + U_{b2} + U_t + U_l$, where U_{bi} $(i = 1,2)$ is the internal strain energy stored in beam i, U_t is the internal strain energy for the partial twist restraint of the deck bending action, and U_l is the internal strain energy for the relative partial lateral restraint of the deck-joint assembly. The load potential energy V consists of two components, i.e., $V = V_{b1} + V_{b2}$, one for each beam.

The internal strain energy stored in beam i due to weak-axis bending, Saint-Venant torsion, and warping torsion takes the following form (Trahair [46])

$$U_{bi} = (1/2)\int_0^{L_b} \left(E_b I_y u_i''^2 + G_b J_b \theta_i'^2 + E_b C_w \theta_i''^2 \right) dz \quad (i = 1, 2) \tag{2}$$

where $E_b = E_{Lb}$ is the beam modulus of elasticity in the longitudinal direction, I_y is the moment of inertia about beam weak-axis, $G_b = G_{Lb}$ is the shear modulus for stresses acting on the plane normal to the longitudinal direction, J_b is the Saint-Venant torsional constant, C_w is the warping constant, L_b is the beam span, and all primes denote differentiation with respect to coordinate z taken along the beam longitudinal axis. For wood beams with rectangular cross-sections, material properties E_b and G_b are taken as the material properties of the wood type used. For doubly symmetric I-section members where the web and flanges have different materials, E_b and G_b are the transformed section properties (Du et al. [5]). The load potential energy for external loads applied at beam i (Trahair [46]) is

$$V_{bi} = \lambda \int_0^{L_b} \left(2M\theta_i u_i'' + qh\theta_i^2 \right) dz \quad (i = 1, 2) \tag{3}$$

where M is the bending moment induced by the reference load q (taken positive when acting downwards), and one recalls that λ is an unknown load multiplier to be obtained from the buckling analysis and h is the height of the loading point above the shear center (taken positive when the loading point is below beam shear center). The first term in Eq. (3) accounts for the destabilizing effect due to strong-axis flexure while the second term accounts for load potential energy gain due to the load offset from the beam shear center. For a given deck board located at a distance z_0 from the

beam end support, and angles of twist $\theta_1(z_0)$ and $\theta_2(z_0)$ the internal strain energy stored in this deck board is

$$U_t^* = \frac{E_d I_d}{L_d} \left\langle \theta_1(z_0) \quad \theta_2(z_0) \right\rangle \begin{bmatrix} 2 & 1 \\ 1 & 2 \end{bmatrix} \begin{Bmatrix} \theta_1(z_0) \\ \theta_2(z_0) \end{Bmatrix} \tag{4}$$

where E_d is the deck modulus of elasticity, I_d is the moment of inertia about the deck board and L_d is the span of deck board. The internal strain energy U_t for the whole deck is simply the summation of the contribution from each deck board which can be approximately written in an integration form as

$$U_t = \sum U_t^* \approx \frac{E_d h_d^3}{12 L_d} \int_0^{L_b} \left\langle \theta_1(z) \quad \theta_2(z) \right\rangle \begin{bmatrix} 2 & 1 \\ 1 & 2 \end{bmatrix} \begin{Bmatrix} \theta_1(z) \\ \theta_2(z) \end{Bmatrix} dz \tag{5}$$

where h_d is the deck board thickness. For a deck board at a distance z_0 from beam end support, the lateral displacements of points *A* and *C* at beams' top (Fig. 1) are expressed in terms of the lateral displacement u_i and angle of twist θ_i as

$$u_A(z_0) = u_1(z_0) + (h_b/2)\theta_1(z_0), \qquad u_C(z_0) = u_2(z_0) + (h_b/2)\theta_2(z_0) \tag{6}$$

where h_b is the beam depth.

The internal strain energy U_l associated with the relative partial lateral restraint provided by the deck to the beams can be characterized by considering the lateral stiffness k of the deck-joint assembly as three springs in tandem (i.e., two springs, each representing the shear stiffness k_j of each joint at the beam-deck interface, and another spring representing the axial stiffness of the deck k_d). Stiffness k relates the relative displacement $u_c - u_A$ between the two beams proportionally to the lateral force $F = k(u_c - u_A)$. Adding the flexibility of the three spring components yields $1/k = 1/k_j + 1/k_d + 1/k_j$, which is solved for the overall stiffness k as

$$k = k_d k_j \big/ \left(2k_d + k_j\right) \tag{7}$$

Assuming $\overline{n}$ nails are installed at each beam-deck joint, each with the shear stiffness k_n, the shear stiffness k_j of the joint is $k_j = \overline{n} k_n$. The stiffness of a single-nail joint k_n can be estimated based on the load-displacement model in CAN/CSA O86 [2]

$$\Delta_n = 0.5 d_F K_m \left(F/F_u\right)^{1.7} \tag{8}$$

where Δ_n is the shear deformation of a single-nail joint, d_F is the nail diameter in millimeter, K_m is the service creep factor accounting for load duration and moisture level, and F_u is the lateral strength resistance as governed by the smallest capacities amongst different failure modes. In the present study, the value $K_m = 1$ is used. The shear stiffness k_n is taken as the initial stiffness from Eq. (8), i.e., gradient that joins the origin and 10% of the lateral strength resistance F_u.

The model that quantifies the deck axial stiffness at the height of beam-deck interface is schematically depicted in Fig. 2 where the deck board is assumed to be subjected to a pair of eccentric loads F acting at the beam-deck interface. The lateral deformation Δ of the deck board is consisted of two components, an axial deformation Δ_1, and another deformation Δ_2 associated with transverse bending, i.e.,

$$\Delta = \Delta_1 + \Delta_2 = FL_d \big/ E_d b h_d + M_d M_0 L_d \big/ E_d I_d \tag{9}$$

where M_d is the bending moment induced by eccentric lateral loads F and is expressed as $M_d = Fh_d/2$, b is deck board width, and M_0 is the moment for unit lateral loads. From the expressions for M_d and M_0, by substituting into Eq. (9), one obtains $\Delta = FL_d/E_d b h_d + Fh_d^2 L_d/4E_d I_d = 4FL_d/E_d b h_d$ and the axial stiffness of the deck board k_d at the height of beam-deck interface is $k_d = E_d b h_d/4L_d$. From the

expression for k_d, by substituting into Eq. (7), one obtains the sought relative lateral stiffness as

$$k = \overline{n}E_d b h_d k_n \big/ \left(2E_d b h_d + 4\overline{n}L_d k_n\right) \tag{10}$$

For example, for a 38 mm by 140 mm deck board spanning 2 m and having a modulus of elasticity of 10,000 MPa, the relative lateral stiffness of a single nail with a 3.66mm diameter at each joint is 1061 kN/m or 7579 kN/m/m (per unit length of deck), while that based on two nails at each joint is 1830 kN/m, or 13073 kN/m/m.

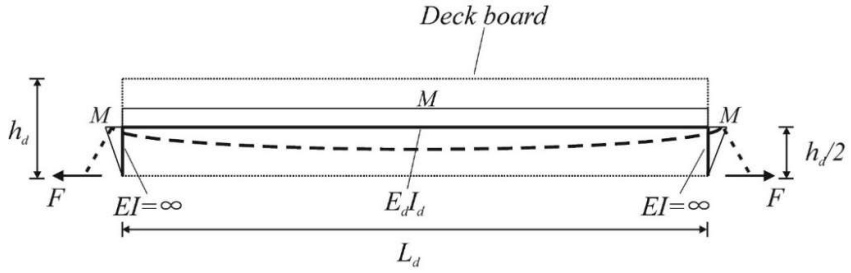

Fig. 2 Deck board deformation due to eccentric lateral loads acting at the deck underside

The corresponding internal strain energy stored in the deck board is

$$U_l^* = \left(k/2\right)\left(u_C - u_A\right)^2 = \left(k/2\right)\left\{u_2\left(z_0\right) - u_1\left(z_0\right) + \left(h_b/2\right)\left[\theta_2\left(z_0\right) - \theta_1\left(z_0\right)\right]\right\}^2 \tag{11}$$

For the whole deck, the internal strain energy is the summation of the energy contributions from all deck boards, which can be approximated in an integral form as

$$U_l = \sum U_l^* \approx \left(\overline{k}/2\right)\int_0^{L_b}\left[u_2 - u_1 + \left(h_b/2\right)\left(\theta_2 - \theta_1\right)\right]^2 dz \tag{12}$$

where the relative lateral stiffness per unit deck width $\overline{k} = k/b$ has been defined. In summary, from Eqs. (2),(3),(5), and (12), by substituting into Eq. (1), one obtains the total potential energy of the twin-beam-deck assembly as

$$\Pi = \frac{1}{2}\int_0^{L_b} E_b I_y \left(u_1''^2 + u_2''^2\right) + G_b J_b \left(\theta_1'^2 + \theta_2'^2\right) + E_b C_w \left(\theta_1''^2 + \theta_2''^2\right)$$
$$+ \left(E_d h_d^{\,3}/3L_d\right)\left(\theta_1^2 + \theta_1\theta_2 + \theta_2^2\right) + \bar{k}\left[u_2 - u_1 + \left(h_b/2\right)\left(\theta_2 - \theta_1\right)\right]^2 \qquad (13)$$
$$+ 2\lambda M\left(\theta_1 u_1'' + \theta_2 u_2''\right) + \lambda q h\left(\theta_1^2 + \theta_2^2\right) dz$$

6. Finite Element Formulation

The Hermitian polynomials are adopted to relate the lateral displacement fields u_i and rotation fields θ_i $(i = 1, 2)$ to the generalized nodal displacements, i.e.

$$u_i(z) = \left\langle L(z)\right\rangle_{1\times 4}^T \left\{u_i\right\}_{4\times 1}, \qquad \theta_i(z) = \left\langle L(z)\right\rangle_{1\times 4}^T \left\{\theta_i\right\}_{4\times 1} \qquad (14)$$

where

$$\left\langle L(z)\right\rangle_{1\times 4}^T = \left\langle \left(1 - 3z^2/l^2 + 2z^3/l^3\right) \quad \left(z - 2z^2/l + z^3/l^2\right) \quad \left(3z^2/l^2 - 2z^3/l^3\right) \quad \left(z^3/l^2 - z^2/l\right)\right\rangle$$

is the vector of Hermitian interpolation functions and l is the element length,

$$\left\langle u_i\right\rangle_{1\times 4}^T = \left\langle u_0 \quad u_0' \quad u_l \quad u_l'\right\rangle_i$$ is the generalized nodal lateral displacement vector,

$$\left\langle \theta_i\right\rangle_{1\times 4}^T = \left\langle \theta_0 \quad \theta_0' \quad \theta_l \quad \theta_l'\right\rangle_i$$ is the generalized nodal angle of twist vector, and subscripts *0* and *l* denote the nodal points of the element. From Eq. (14), by substituting into Eq. (13), one obtains

$$\Pi = (1/2)\left\langle U\right\rangle_{1\times 16}^T \left[\left[K_e\right] - \lambda\left[K_g\right]\right]_{16\times 16} \left\{U\right\}_{16\times 1} \qquad (15)$$

where $\left\langle U\right\rangle^T = \left\langle \left\langle u_1\right\rangle_{1\times 4}^T \quad \left\langle u_2\right\rangle_{1\times 4}^T \quad \left\langle \theta_1\right\rangle_{1\times 4}^T \quad \left\langle \theta_2\right\rangle_{1\times 4}^T\right\rangle$ and the elastic stiffness matrix $\left[K_e\right] = \left[K_b\right] + \left[K_t\right] + \left[K_l\right]$ has three contributions: $\left[K_b\right]$ which characterizes the beam stiffness matrix, $\left[K_t\right]$ which characterizes partial twist restraint, and $\left[K_l\right]$ which characterize the relative partial lateral restraint and are given by

$$[K_b]=\left[\begin{array}{c|c|c|c} E_bI_y[B_1] & [0] & [0] & [0] \\ \hline [0] & E_bI_y[B_1] & [0] & [0] \\ \hline [0] & [0] & E_bC_w[B_1]+G_bJ_b[B_2] & [0] \\ \hline [0] & [0] & [0] & E_bC_w[B_1]+G_bJ_b[B_2] \end{array}\right]_{16\times16} \tag{16}$$

$$[K_t]=\frac{E_dh_d{}^3}{6L_d}\left[\begin{array}{c|c|c|c} [0] & [0] & [0] & [0] \\ \hline [0] & [0] & [0] & [0] \\ \hline [0] & [0] & 2[B_3] & [B_3] \\ \hline [0] & [0] & [B_3]^T & 2[B_3] \end{array}\right]_{16\times16} \tag{17}$$

$$[K_l]=\frac{\bar{k}}{4}\left[\begin{array}{c|c|c|c} 4[B_3] & -4[B_3] & 2h_b[B_3]^T & -2h_b[B_3]^T \\ \hline -4[B_3]^T & 4[B_3] & -2h_b[B_3]^T & 2h_b[B_3]^T \\ \hline 2h_b[B_3] & -2h_b[B_3] & h_b{}^2[B_3] & -h_b{}^2[B_3] \\ \hline -2h_b[B_3] & 2h_b[B_3] & -h_b{}^2[B_3]^T & h_b{}^2[B_3] \end{array}\right]_{16\times16} \tag{18}$$

354 The geometric stiffness matrix $[K_g]$ takes the following form

$$[K_g]=\left[\begin{array}{c|c|c|c} [0] & [0] & -[B_4]^T & [0] \\ \hline [0] & [0] & [0] & -[B_4]^T \\ \hline -[B_4] & [0] & -h[B_5] & [0] \\ \hline [0] & -[B_4] & [0] & -h[B_5] \end{array}\right]_{16\times16} \tag{19}$$

355 and submatrices $[B_1],[B_2],[B_3],[B_4],[B_5]$ are defined as

356 $[B_1]=\int_0^l\{L''(z)\}_{4\times1}\langle L''(z)\rangle_{1\times4}^T dz,\ [B_2]=\int_0^l\{L'(z)\}_{4\times1}\langle L'(z)\rangle_{1\times4}^T dz,$

357 $[B_3]=\int_0^l\{L(z)\}_{4\times1}\langle L(z)\rangle_{1\times4}^T dz,\ [B_4]=\int_0^l M(z)\{L(z)\}_{4\times1}\langle L''(z)\rangle_{1\times4}^T dz$ and

358 $[B_5]=\int_0^l q(z)\{L(z)\}_{4\times1}\langle L(z)\rangle_{1\times4}^T dz$. From Eq. (15), by evoking the stationarity of the

359 total potential energy, i.e., $\delta\Pi=0$, one obtains

$$\left([K_e]-\lambda[K_g]\right)_{16\times16}\{U\}_{16\times1}=\{0\}_{16\times1} \tag{20}$$

7. Results

A wooden twin-beam-deck assembly of common wood properties and practical dimensions is chosen as a reference case to be used to assess the validity of the present finite element solution through comparisons to the predictions of a model based on the commercial software ABAQUS. The present finite element is then used to conduct a parametric study by varying one parameter at a time from the reference case and observing the critical moments and buckling mode shapes. For verification, the transverse loads are applied at the beam shear center while for the parametric study, unless specified otherwise, the transverse loads are applied at deck centerline.

The reference beam span is taken as 6m and the deck span is taken as 2 m. The beams are assumed to be glue-laminated Spruce-Lodgepole Pine-Jack Pine 20f-EX with 570 mm in depth and 80 mm in width. The modulus of elasticity and shear modulus are assumed to be 10,300 MPa and 474 MPa, respectively. The nominal bending moment resistance based on material failure is 270 kNm. The deck boards are assumed to be Spruce-Pine-Fir No. 2 grade and are 38 mm thick and 140 mm wide with a modulus of elasticity of 10,000 MPa. All the material properties mentioned above are based on CAN/CSA O86 [2] and FPL [43]. Two 3.66 mm nails are assumed to be installed at each beam-deck intersection. Both uplift and downward buckling loads are investigated.

7.1 Details of ABAQUS model

The finite-element program ABAQUS was used to conduct an eigenvalue buckling analysis of the twin-beam-deck assembly. The two-node B31OS element was used to model the twin beams. Each node has seven degrees of freedom (i.e., three translations, three rotations, and one warping deformation). The element accounts for shear deformation only due to bending but ignores shear deformation induced by warping. Two types of elements were chosen to capture the twist restraint of the deck and the

relative lateral restraint of the deck-joint assembly. The B31 element was used to model the flexural stiffness of the deck boards. The B31 element has two nodes with six degrees of freedom per node (i.e., three translations and three rotations). The two-node SPRING2 spring element was employed to simulate the partial relative lateral restraining action between the top of both beams for the deck-joint assembly. Fig. 3 shows the twin-beam-deck model developed, with B31OS elements depicted at the centroidal axes of twin beams, B31 elements at the deck board centerlines, and SPRING2 elements spanning between the top of twin beams. The number of B31OS elements in each beam was chosen to be consistent with the number of deck boards. Each deck node (lying on line 2 or 5 in Fig. 3) was rigidly tied to the corresponding centroidal node (on line 1 or 4). Also, each spring node (on line 3 or 6) was tied to the corresponding centroidal node (on line 1 or 4). Both rigid links were defined using the BEAM type multi-point constraint (*MPC) feature in ABAQUS.

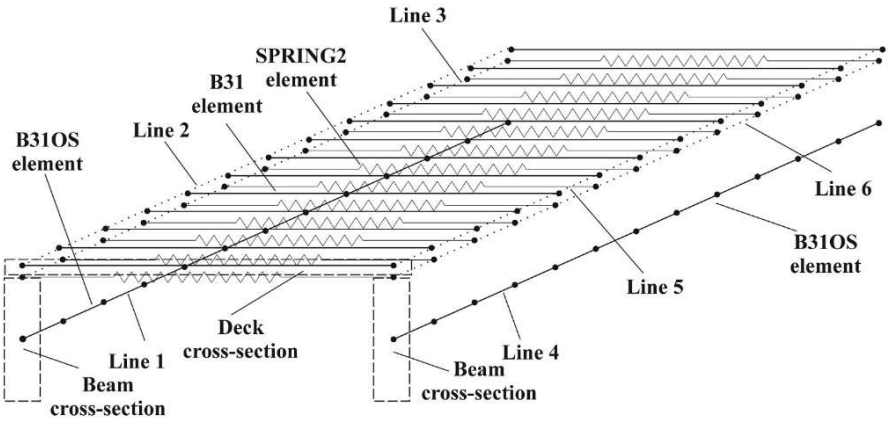

Fig. 3 ABAQUS twin-beam-deck model

7.2 Mesh convergence study

For the present FEA model, a mesh convergence study is performed for uniform moment loading (Fig. 4a), UDL (Fig. 4c), and mid-span concentrated loads (Fig. 4e). Systems with transverse loads applied at the beam shear center are observed to have equal critical positive moments (tension at the beams' bottom) and negative moments.

Thus, only the magnitudes of the moments are presented. Among all three load types investigated, the present FEA results are observed to converge from above. No more than 10 beam elements are found to be needed to attain convergence.

7.3 Verification

For uniform moment loading (Fig. 4a), the critical moments determined by the present FEA solutions yield a value of 193 kNm, compared with a slightly lower value of 192 kNm predicted from ABAQUS. This is attributed to the fact that the ABAQUS B31OS elements incorporate shear deformation effects due to flexure and thus provide a more flexible representation of the system. The mode shapes as predicted by both solutions are found in close agreement (Fig. 4b).

For UDL (Fig. 4c), the present FEA predicts a critical moment of 212.1 kNm which is slightly higher than 211.8 kNm as predicted by the ABAQUS and the predicted mode shapes nearly coincide (Fig. 4d). Similar observations are found for mid-span concentrated loading (Fig. 4e, Fig. 4f). The above comparisons show good agreement between the present FEA model and ABAQUS. The present FEA model, thus verified, is subsequently used to investigate the effects of various parameters on critical moments.

7.4 Effects of beam and deck spans

The effects of beam and deck spans are illustrated in Fig. 4g and Fig. 4h. When the beam span is increased from 2 m to 10 m (Fig. 4g), the buckling capacity for upward UDL as predicted by the present FEA decreases from 412 kNm to 204 kNm. In contrast, for downward UDL, the critical moment declines slightly from 219 kNm to 198 kNm. For both upward and downward UDL, as the deck span is increased from 1 m to 5 m, Fig. 4h shows a consistent decline in buckling capacity. The critical moment corresponding to the case of a 5 m deck span is roughly half of the capacity of the case of a 1 m deck span.

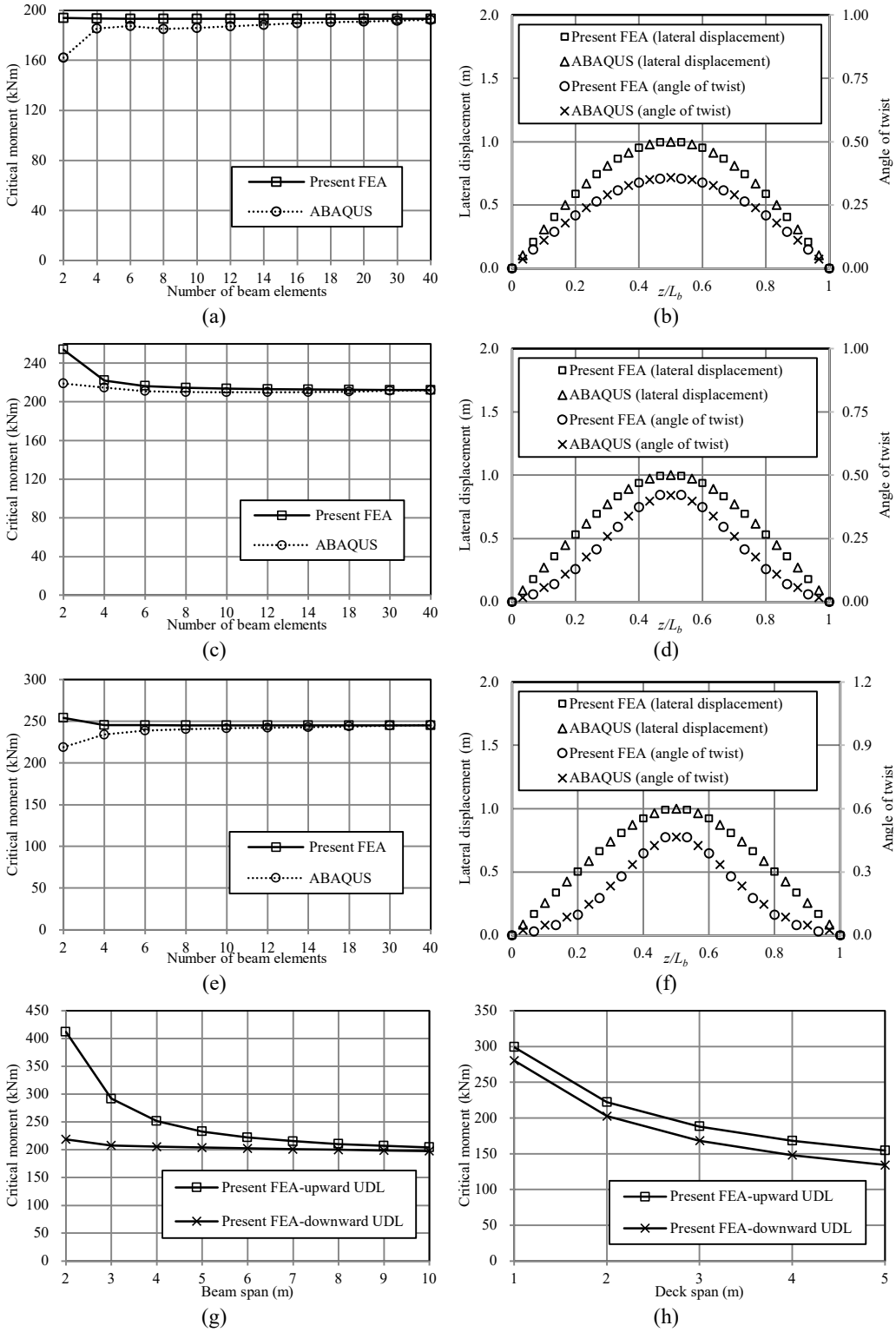

Fig. 4 (a) Convergence study for uniform moments, (b) mode shapes for uniform moments, (c) convergence study for UDL, (d) mode shapes for UDL, (e) convergence study for mid-span concentrated loads, (f) mode shapes for mid-span concentrated loads, (g) critical moments for UDL with varying beam span, (h) critical moments for UDL with varying deck span

7.5 Effect of relative lateral stiffness of the deck-joint assembly

Fig. 5a shows the critical moments as a function of the relative lateral stiffness per unit deck width $\bar{k}$ for a beam-deck system subjected to UDL acting at the height of beam shear center. Two beam spans were investigated, i.e., 2 m and 6 m. For the 2 m span, the critical moments for downward loading increase with $\bar{k}$ up to 100 kN/m/m, after which the critical moment remains constant at 301 kNm. In contrast, the critical moment for upward loading remains constant at 250 kNm irrespective of the magnitude of $\bar{k}$. For the 6 m span, the critical moments for upward and downward UDL increase as $\bar{k}$ is increased. The increase in critical moments for downward loading is faster than that of upward loading, resulting in a higher buckling capacity for a certain stiffness range. The critical moments for upward and downward loading are found equal with a magnitude of 212 kNm when $\bar{k}$ exceeds the threshold value of 45.3 kN/m/m. For the reference deck-joint assembly, $\bar{k}$ corresponding to a single nail per joint is 7579 kN/m/m while that based on two nails per joint is 13073 kN/m/m. Both values are depicted by the vertical lines on Fig. 5a. For the problem examined, both stiffness values far exceed the threshold stiffness value, resulting in identical critical moment for upward and downward loading. Further investigation on beam spans of 4 m and longer suggests similar conclusions. Such results were omitted from Fig. 5a, to avoid clutter. The present example suggests that a beam-deck connection with a single nail provides enough lateral stiffness to develop their peak critical moments.

7.6 Effect of lateral restraint height

For the reference twin-beam-deck assembly subjected to UDL, the relative lateral restraint of the deck-joint assembly is hypothetically moved from the beam shear center to the deck centerline and the corresponding critical moments are presented in Fig. 5b.

458 Two categories of restraint stiffness were considered: below and above the threshold
459 value. Considered was the relative lateral stiffness per unit deck width $\bar{k} = 10$ kN/m/m,
460 a value below the threshold stiffness (discussed in the previous section). For upward
461 loading, the critical moments are observed to decrease from 205 kNm to 185 kNm as
462 the restraint moves from the shear center to the deck centerline. In contrast, for
463 downward loading, the critical moments are observed to increase from 168 kNm to 189
464 kNm. The results suggest that the restraint height has a moderate effect on the critical
465 moments for $\bar{k}$ below the threshold value. For a relative lateral stiffness above the
466 threshold stiffness ($\bar{k} = 13,073$ kN/m/m for a two-nail connection), the critical moments
467 corresponding to upward and downward loading remain constant at 222 kNm and 203
468 kNm, respectively. Insight on the above observations can be provided by examining the
469 associated mode shapes. For a relative lateral stiffness below the threshold value, the
470 modes are observed to be symmetric (i.e., $u_1 = -u_2$ and $\theta_1 = -\theta_2$). Thus, the internal
471 strain energy for the partial lateral restraint (i.e., Eq.(12)) is non-zero and is influenced
472 by the restraint height. In contrast, when the relative lateral stiffness is beyond the
473 threshold value, the modes become anti-symmetric (i.e., $u_1 = u_2$ and $\theta_1 = \theta_2$), causing
474 Eq. (12) to vanish, thus eliminating the dependence of the solution on the restraint
475 height.

476 **7.7 Effects of partial relative lateral and twist restraints**

477 The critical moments for the reference twin-beam-deck assembly subjected to UDL
478 applied at the deck centerline are examined for various restraint scenarios: (1) partial
479 relative lateral and twist restraints included, (2) partial twist restraint with no relative
480 partial lateral restraint, (3) relative partial lateral restraint with no partial twist restraint,
481 and (4) no restraints. For downward loading (Fig. 5c), the contribution of the relative

partial lateral restraint is illustrated by the gap between the upper solid line and the dotted line. The contribution of the restraint grows as the span increases from 2 m to 6 m, after which the restraint contributes a steady 40% of the total capacity. Interestingly, the results corresponding to twin-beams with relative partial lateral restraint alone (no twist restraint) are observed to coincide with those of no restraints. This suggests that the presence of relative lateral restraint alone between identical beams identically loaded provides no LTB capacity increase. The results also suggest that the buckling capacities with lateral and twist restraints are 1.6 times (beam with 2 m span) to 6 times (beam with 10 m span) higher than those without restraints. Similar conclusions can be drawn from the case of upward UDL loading (Fig. 5d).

7.8 Effect of load position

Three load positions are considered: (1) Deck centerline, (2) beam shear center and (3) beam bottom. The critical moments are examined for beam spans of 4, 6, and 8 m and deck spans of 1, 3, and 5 m and results are presented in Tables 1 and 2, respectively. For downward loading, because of the destabilizing effect induced by deck centerline loading, the buckling capacities are observed to be lower than those based on beam shear center loading. The percentage decreases are 10.1%, 4.25% and 2.44% for 4, 6 and 8 m span, respectively. In contrast, loads applied at beam bottom is found to be associated with a stabilizing effect which increases the buckling capacity. The percentage increases are 9.65%, 4.72% and 2.44% for beam spans of 4, 6 and 8 m, respectively. For upward loading, an opposite trend is observed where deck centerline loading is found to correspond to the highest critical moments. The results in Table 1 suggest that the load position effect is more pronounced in short span beams. Table 2 suggests that the load position effect remains relatively steady (between 3%-7%) as the deck span is varied from 1 m to 5 m.

7.9 Effect of beam span on a two-span continuous twin-beam-deck system

Fig. 6a and Fig. 6b show the buckling capacity of a twin-beam-deck system with two-span continuous beams under UDL and mid-span concentrated loads applied to both spans. For downward loading, the critical moments at mid-span remain nearly constant at 200 kNm and are found to be insensitive to the span. In contrast, for upward loading, critical moments are found to decrease as the span is increased from 4 to 10m. This trend is consistent with the observations from single-span beams. Table 3 provides a comparison of the critical moments for single-span and two-span twin-beam-deck systems with a UDL applied at the deck centerline. The results suggest that, in general, the critical moments for two-span twin-beam-deck assemblies are slightly higher than those based on single-span assemblies of the same span.

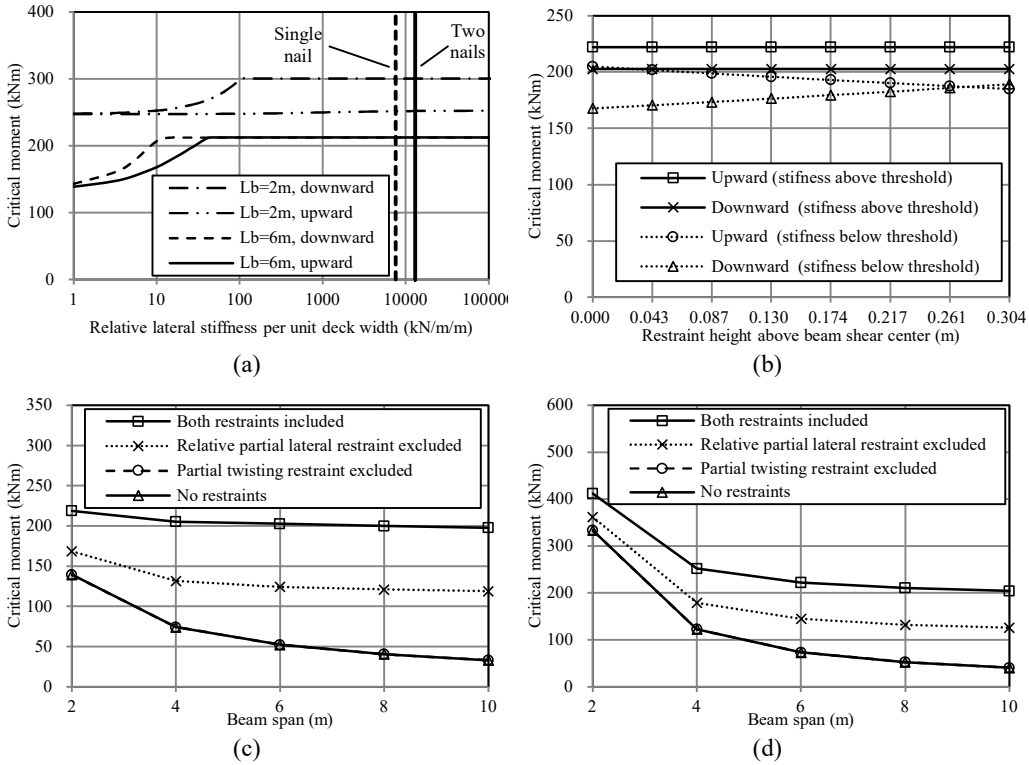

Fig. 5 (a) Buckling capacity for (a) different lateral stiffness, (b) different lateral restraint height; Buckling capacity as influenced by inclusion/exclusion of partial lateral and twist restraints under (c) downward UDL with varying beam span, (d) upward UDL with varying beam span

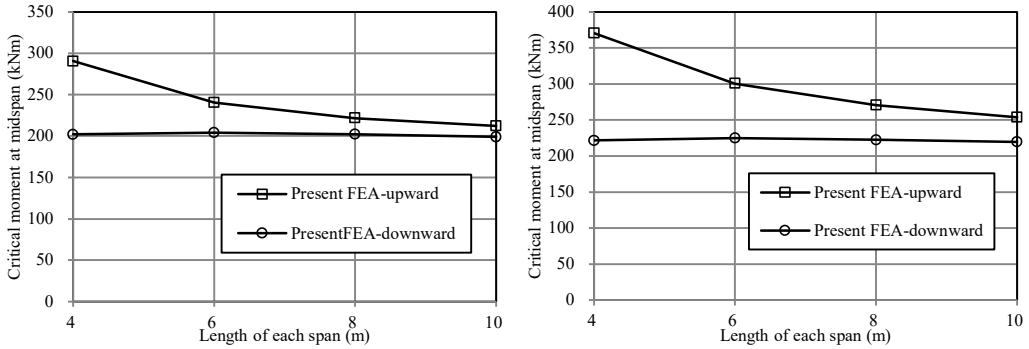

522 **Fig. 6** Buckling capacity for two-span twin-beam-deck systems with varying spans under (a)
523 UDL, (b) mid-span concentrated loads

524

525

526

527

528

529

530 Table 1 Load position effect for different beam spans

Beam span (m)	Load position	Downward UDL		Upward UDL	
		Critical moment (kNm)	Difference	Critical moment (kNm)	Difference
4	Deck centerline	205	-10.1%	252	10.5%
	Beam shear center	228	/	228	/
	Beam bottom	250	9.65%	176	-22.8%
6	Deck centerline	203	-4.25%	222	4.72%
	Beam shear center	212	/	212	/
	Beam bottom	222	4.72%	203	-4.25%
8	Deck centerline	200	-2.44%	210	2.44%
	Beam shear center	205	/	205	/
	Beam bottom	210	2.44%	200	-2.44%

531

532 Table 2 Load position effect for different deck spans

Deck span (m)	Load position	Downward UDL		Upward UDL	
		Critical moment (kNm)	Difference	Critical moment (kNm)	Difference
1	Deck centerline	280	-3.21%	299	3.31%
	Beam shear center	290	/	290	/
	Beam bottom	299	3.10%	281	-3.01%
3	Deck centerline	168	-5.46%	188	5.73%
	Beam shear center	178	/	178	/

	Beam bottom	188	5.37%	169	-5.12%
5	Deck centerline	134	-6.84%	155	7.29%
	Beam shear center	144	/	144	/
	Beam bottom	154	6.82%	135	-6.42%

Table 3 Comparison between single-span and two-span twin-beam-deck systems

Beam span or length of each span (m)	Downward UDL			Upward UDL		
	Single-span beams (kNm) [1]	Two-span beams (kNm) [2]	[2]/[1]	Single-span beams (kNm) [3]	Two-span beams (kNm) [4]	[4]/[3]
4	205	202	0.985	252	291	1.12
6	203	204	1.01	222	240	1.08
8	200	202	1.01	210	222	1.06
10	198	199	1.01	204	212	1.04

8. Conclusions

A finite element formulation was developed for predicting LTB capacity of twin beams continuously braced by deck boards. The solution captures the continuous relative partial lateral restraint provided by the stiffness of deck-joint assembly and the partial twist restraint provided by the deck bending stiffness. The results based on the present solution are observed to be in close agreement with those based on ABAQUS while involving a minimal computational effort. For wooden twin-beam-deck systems investigated in the present study, the following observations were made:

1. The combined actions of continuous partial relative lateral and twist restraints significantly increase LTB capacity. Compared with unrestrained beams, the capacity increase can be as much as six folds. However, the provision of relative lateral restraint alone was found ineffective in increasing the buckling capacity.
2. As the beam span is increased from 2 m to 10 m, the buckling capacity for upward loading decreases by half while that based on downward loading remains

essentially constant. The buckling capacity for both upward and downward loads declines significantly as the deck span is increased.

3. The load position greatly influences the buckling capacity for beam-deck systems with short beam spans. Numerical results show that the buckling capacity can be influenced by 10% to 23% when the load is moved away from beam shear center. For beams with intermediate and long spans, the load position effect is below 5%.
4. The height of lateral restraint has no effect on the buckling capacity when the relative lateral stiffness of the deck-joint assembly exceeds a threshold value.
5. A single nail connecting the beam to a 38 mm thick deck board provides lateral stiffness that far exceeds the stiffness threshold to achieve maximum buckling capacity. Additional measures to strengthen the beam-deck connections will not lead to an increase in the buckling capacity.
6. The trend between beam span and buckling capacity for two-span twin-beam-deck systems is similar to that of single span systems. The buckling capacity for two-span systems is comparable to that of single-span systems with the same span.

Notation

A, B, C, D	nodes located at beams upside or deck underside;
A_i, A_i'	amplitudes of lateral displacement functions;
B_i, B_i'	amplitudes of the angle of twist functions;
$[B_1], [B_2], [B_3], [B_4], [B_5]$	submatrices of the elastic and geometric stiffness matrices;
b	deck board width;
C_w	warping constant;
d_F	nail diameter;
E_b, E_d	modulus of elasticity of beam and deck, respectively;
E_L, E_T, E_R	modulus of elasticity in longitudinal, tangential, radial directions
F	lateral load at the beam-deck intersection;
F_u	lateral strength resistance;
G_b	shear modulus of the beam;
G_T	shear modulus in transverse direction;

580 G_{LR} shear modulus about longitudinal and radial direction;
581 G_{LT} shear modulus about longitudinal and tangential direction;
582 G_{RT} shear modulus about radial and tangential direction;
583 h distance between loading point and beam shear center;
584 h_b, h_d depth of beam and deck, respectively;
585 I_d moment of inertia of a deck board in the strong-axis;
586 I_y moment of inertia about beam weak-axis;
587 J_b beam Saint-Venant torsional constant;
588 K_m service creep factor;
589 $[K_b]$ beam stiffness matrix;
590 $[K_e]$ elastic stiffness matrix;
591 $[K_g]$ geometric stiffness matrix;
592 $[K_l]$ stiffness matrix for the relative lateral restraint;
593 $[K_t]$ stiffness matrix for the twist restraint;
594 k relative lateral stiffness;
595 $\overline{k}$ relative lateral stiffness per unit deck width;
596 k_d axial stiffness of deck board at the height of beam top;
597 k_j shear stiffness at the beam-deck joint;
598 k_n shear stiffness of a single-nail joint;
599 L_b, L_d beam and deck span, respectively;
600 $\langle L(z) \rangle^T$ Hermitian polynomials;
601 M reference strong-axis moment;
602 M_{cr} critical moment
603 M_d deck strong-axis moment under eccentric lateral loads;
604 M_{e1}, M_{e2} deck board end moments;
605 M_0 deck strong-axis moment under unit eccentric lateral loads;
606 n integer;
607 $\overline{n}$ number of nails at each joint;
608 $q(z)$ reference transverse load;
609 U internal strain energy;
610 U_{bi} internal strain energy in beam i;
611 U_l internal strain energy for the relative partial lateral restraint;
612 U_t internal strain energy for the partial twist restraint;
613 U_l^* internal strain energy for relative partial lateral restraint in one deck board;
614 U_t^* internal strain energy for the partial twist restraint in one deck board;
615 u_A, u_C lateral displacements for nodes A and C, respectively;
616 u_i lateral displacement of beam i;
617 $\langle u_i \rangle$ generalized nodal lateral displacement vector;

618	V	load potential energy;
619	V_{bi}	load potential energy for beam i;
620	$v_p(z)$	prebuckling vertical displacement;
621	x, y, z	Cartesian coordinates;
622	z_0	distance from a given deck board to beam end-support;
623	Δ	deck lateral deformation;
624	Δ_1	deck axial deformation;
625	Δ_2	deck axial deformation due to transverse bending;
626	Δ_n	joint deformation of a single-nail joint;
627	θ_i	angle of twist of beam i;
628	$\langle \theta_i \rangle$	generalized nodal angel of twist vector;
629	λ	load multiplication factor;
630	μ	Poisson's ratio;
631	μ_{LR}	Poisson's ratio in longitudinal and radial direction;
632	μ_{LT}	Poisson's ratio in longitudinal and tangential direction;
633	μ_{RT}	Poisson's ratio in radial and tangential direction;
634	Π	total potential energy.

635 ## Acknowledgments

636 The authors gratefully acknowledge funding from the Natural Sciences and

637 Engineering Research Council (NSERC) of Canada to the second and third authors.

638 ## References

639 [1] American Wood Council. National design specification (NDS) for wood construction. Leesburg, VA,

640 USA 2015.

641 [2] Canadian Standard Association (CSA). Engineering design in wood O86-14. Mississauga, ON,

642 Canada 2014.

643 [3] European Committee for Standardization. Eurocode 5: Design of timber structures-Part 1-1: General

644 common rules and rules for buildings. Brussels, Belgium 2004.

645 [4] Du Y, Mohareb M, Doudak D. Lateral torsional buckling of twin-beam deck assemblies under wind

646 uplift—Sway versus non-sway models. Proceedings of the World Conference in Timber Engineering,

647 Vienna, Austria, 2016, 22–25.

648 [5] Du Y, Mohareb M, Doudak G. Nonsway Model for Lateral Torsional Buckling of Wooden Beams

649 under Wind Uplift. Journal of Engineering Mechanics 2016; 142:04016104.

650 [6] Hooley RF, Madsen B. Lateral stability of glued laminated beams. Journal of the Structural Division
651 1964; 90:201–218.
652 [7] Hindman DP, Manbeck HB, Janowiak JJ. Measurement and prediction of lateral torsional buckling
653 loads of composite wood materials: rectangular sections. Forest Products Journal 2005; 55:42.
654 [8] Hindman DP, Manbeck HB, Janowiak JJ. Measurement and prediction of lateral torsional buckling
655 loads of composite wood materials: I-joist sections. Forest Products Journal 2005; 55:43.
656 [9] Burow JR, Manbeck HB, Janowiak JJ. Lateral stability considerations for composite wood I-joists.
657 2005 ASAE Annual Meeting, American Society of Agricultural and Biological Engineers; 2005, p. 1.
658 [10] Burow JR, Manbeck HB, Janowiak JJ. Lateral stability of composite wood I-joists under
659 concentrated-load bending. Transactions of the ASABE 2006; 49:1867–1880.
660 [11] Xiao Q, Doudak G, Mohareb M. Numerical and experimental investigation of lateral torsional
661 buckling of wood beams. Eng Struct 2017; 151: 85-92.
662 [12] St-Amour R. Lateral Torsional Buckling of Wood I-Joist. Master of Applied Science Thesis. Ottawa,
663 ON, Canada: Department of Civil Engineering, University of Ottawa; 2016.
664 [13] Hu Y, Mohareb M, Doudak G. Effect of Eccentric Lateral Bracing Stiffness on Lateral Torsional
665 Buckling Resistance of Wooden Beams. International Journal of Structural Stability and Dynamics
666 2017:1850027.
667 [14] Hu Y, Mohareb M, Doudak G. Lateral Torsional Buckling of Wooden Beams with Midspan Lateral
668 Bracing Offset from Section Midheight. Journal of Engineering Mechanics 2017;143:04017134.
669 [15] Zahn JJ. Lateral stability of deep beams with shear-beam support. U.S.D.A. Forest Service Research
670 Paper FPL 43, 1965.
671 [16] Jenkinson PM, Zahn JJ. Lateral stability of beam and deck structure. J Struct Div 1972; 98:599-609.
672 [17] Zahn JJ. Lateral stability of wood beam-and-deck systems. J Struct Div 1973; 99:1391-408.
673 [18] Vlasov V. Thin-walled elastic beams, 2nd ed. Israel Program for Scientific Translations. Jerusalem,
674 Israel 1961.
675 [19] Pincus G, Fisher GP. Behavior of diaphragm-braced columns and beams. J Struct Div 1966; 92:323-
676 70.
677 [20] Errera SJ, Pincus G, Fisher GP. Columns and beams braced by diaphragms. J Struct Div
678 1967;93:295-318.

679 [21] Apparao T. Problems in structural diaphragm bracing. Cornell University, School of Civil
680 Engineering, 1968.
681 [22] Hancock GJ, Trahair NS. Finite element analysis of the lateral buckling of continuously restrained
682 beam-columns. Institution of Engineers (Australia) Civ Eng Trans 1978.
683 [23] Trahair N. Elastic lateral buckling of continuously restrained beam-columns. The profession of a
684 civil engineer 1979:61-73.
685 [24] Assadi M, Roeder CW. Stability of continuously restrained cantilevers. J Eng Mech 1985; 111:1440-
686 56.
687 [25] Albert C, Dawe J. Buckling of continuous steel girders with flange restraint. Can J Civ Eng 1990;
688 17:121-8.
689 [26] Khelil A, Larue B. Simple solutions for the flexural-torsional buckling of laterally restrained I-
690 beams. Eng Struct 2008; 30:2923-34.
691 [27] Pekoz T, Soroushian P. Behavior of C- and Z-purlins under wind uplift. In: Sixth international
692 specialty conference on cold-formed steel structures, St Louis, MO; 1982.
693 [28] Sokol L. Stability of cold formed purlins braced by steel sheeting. Thin-walled struct 1996; 25:247-
694 68.
695 [29] Lucas R, Al-Bermani F, Kitipomchai S. Modelling of cold-formed purlin-sheeting systems—Part 1:
696 Full model. Thin-Walled Struct 1997; 27:223-43.
697 [30] Lucas R, Al-Bermani F, Kitipornchai S. Modelling of cold-formed purlin-sheeting systems—Part 2:
698 Simplified model. Thin-Walled Struct 1997; 27:263-86.
699 [31] Ye Z, Kettle RJ, Li L, Schafer BW. Buckling behavior of cold-formed zed-purlins partially
700 restrained by steel sheeting. Thin-walled struct 2002; 40:853-64.
701 [32] Chu X, Kettle R, Li L. Lateral-torsion buckling analysis of partial-laterally restrained thin-walled
702 channel-section beams. J Constr Steel Res 2004; 60:1159-75.
703 [33] Li L. Lateral–torsional buckling of cold-formed zed-purlins partial-laterally restrained by metal
704 sheeting. Thin-walled struct 2004; 42:995-1011.
705 [34] Chu X, Rickard J, Li L. Influence of lateral restraint on lateral-torsional buckling of cold-formed
706 steel purlins. Thin-walled struct 2005; 43:800-10.
707 [35] Basaglia C, Camotim D, Gonçalves R, Graça A. GBT-based assessment of the buckling behaviour
708 of cold-formed steel purlins restrained by sheeting. Thin-walled struct 2013; 72:217-29.

709 [36] Nethercot DA, Trahair NS. Design of diaphragm-braced I-beams. J Struct Div 1975; 101:2045-61.
710 [37] Errera SJ, Apparao TV. Design of I-shaped beams with diaphragm bracing. J Struct Div 1976;
711 102:769-81.
712 [38] Trahair N, Nethercot D. Bracing requirements in thin-walled structures. Elsevier Applied Science
713 Publishers, Developments in Thin-Walled Structures 1984:2:93-130.
714 [39] Lawson R, Nethercot D. Lateral stability of I-beams restrained by profiled sheeting. The Struct Engr
715 1985; 63:3-13.
716 [40] Helwig TA, Frank KH. Stiffness requirements for diaphragm bracing of beams. J Struct Eng 1999;
717 125:1249-56.
718 [41] Helwig TA, Yura JA. Shear diaphragm bracing of beams. I: Stiffness and strength behavior. J Struct
719 Eng 2008; 134:348-56.
720 [42] Helwig TA, Yura JA. Shear diaphragm bracing of beams. II: Design requirements. J Struct Eng
721 2008; 134:357-63.
722 [43] Forest Products Laboratory (FPL). Wood Handbook-Wood as an Engineering Material. Madison,
723 USA 2010.
724 [44] Isopescu D, Stanila O, Astanei I. Analysis of Wood Bending Properties on Standardized Samples
725 and Structural Size Beams Tests. Buletinul Institutului Politehnic Din Lasi Sectia Constructii, Arhitectura
726 2012; 58:65.
727 [45] Xiao Q, Doudak G, Mohareb M. Lateral torsional buckling of wood beams: FEA-modelling and
728 sensitivity analysis. WCTE, Quebec 2014:1–8.
729 [46] Trahair NS. Flexural–torsional buckling of structures. London, UK: E & FN Spon; 1993.
730